Estuaries and Coasts (2025) 48:36
https://doi.org/10.1007/s12237-024-01473-1

Tidal Flooding Contributes to Eutrophication: Constraining Nonpoint Source Inputs to an Urban Estuary Using a Data-Driven Statistical Model

Alfonso Macías-Tapia[1,2] · Margaret R. Mulholland[1] · Corday R. Selden[1,3] · Sophie Clayton[1,4] · Peter W. Bernhardt[1] · Thomas R. Allen[5]

Received: 4 May 2024 / Revised: 18 November 2024 / Accepted: 2 December 2024

Abstract
In coastal urban areas, tidal flooding brings water carrying nutrients and particles back from land to estuarine and coastal waters. A statistical model to predict nutrient loads during tidal flooding events can help estimate nutrient loading from previous and future flooding events and adapt nutrient reduction strategies. We measured concentrations of dissolved inorganic nitrogen and phosphorus in floodwater at seven sentinel sites during 15 tidal flooding events from January 2019 to September 2020. The study area was the Lafayette River watershed in Norfolk, VA, USA, which is prone to tidal flooding and is predicted to experience more frequent and intense flooding in the future. We calculated the difference in dissolved inorganic nitrogen (ΔDIN) or phosphorus (ΔDIP) concentrations between floodwater and those measured in the estuary prior to tidal flooding for each sentinel site and flooding event. We calculated the correlations between ΔDIN and ΔDIP with corresponding data on precipitation, wind, flooding intensity, average estuarine nutrient concentrations, population density, income, land elevation, land use, and land coverage. Using the variables with the highest R^2 values for the linear regression with either ΔDIN or ΔDIP, we built multi-variable random forest regression models. ΔDIN showed the strongest correlations with floodwater nutrient concentrations, water level, and water temperature. ΔDIP also had a strong correlation with floodwater nutrient concentrations and water temperature, but had also a strong correlation wind speed. Models indicated that inputs per flooding event ranged from − 5000 to 7500 kg N, for DIN, while those for DIP ranged from 2000 to 23,000 kg P, with net inputs of > 5000 kg N and > 100,000 kg P, respectively. Removing the dissolved nutrient concentration in floodwater variables from the models, we were able to calculate loads from events that occurred all the way back to 1946. Predicted DIN load per single flooding event ranged from ~ 0 to 1.5×10^5 kg N and showed a significant linear regression with time. Predicted DIP load estimates per single flooding event ranged from $> -1.0 \times 10^5$ to $< 1.5 \times 10^5$ kg P, with a significant positive trend over time. The positive trend in these load values over time shows that they have and will continue to be an increasing problem for the water quality of the local water systems. These results indicate that further action should be taken to control the input of dissolved nutrients during tidal flooding events in urban coastal areas.

Keywords Tidal flooding · Nutrients · Nonpoint source · Eutrophication · Citizen-science · Statistical model

Communicated by Lijun Hou

✉ Alfonso Macías-Tapia
a_maciast@hotmail.com

1 Department of Ocean and Earth Sciences, Old Dominion University, Norfolk, VA, USA

2 Office of Education, National Oceanic and Atmospheric Administration, Silver Spring, Washington, MD, USA

3 Department of Marine and Coastal Sciences, Rutgers, The State University of New Jersey, New Brunswick, NJ, USA

4 Ocean BioGeosciences, National Oceanography Centre, Southampton, UK

5 Department of Political Science & Geography, Old Dominion University, Norfolk, VA, USA

Introduction

Nutrient pollution poses a significant environmental, social, and economic risk to coastal communities around the globe (Cabral et al. 2019; Malone and Newton 2020). The nutrient imbalance can cause the proliferation of harmful algae, which can affect humans in direct contact with contaminated waters or indirectly by consuming affected fisheries (Berdalet et al. 2016). Nutrient inputs can come from point (e.g., the end of a pipe) and nonpoint sources (e.g., runoff; Sabo et al. 2022; Yadav and Pandey 2017); the former are better constrained as sampling need only be conducted at a discharge point (Bouraoui and Grizzetti 2011; Tuholske et al. 2021). Because nonpoint sources of nutrients can be spatially diffuse and temporally variable, often driven by episodic meteorological or other events, they are difficult to quantify (Brown and Froemke 2012). The statistical (e.g., regression) models used to calculate nonpoint source nutrient loads are generally based on only a few measurements that are then applied to heterogeneous systems (Zou et al. 2020; Adu and Kumarasamy 2018) leading to large uncertainties.

Due to sea level rise, many coastal areas around the world are already experiencing increased tidal flooding, and this trend is projected to continue or even accelerate in the decades to come (Nicholls and Cazenave 2010). During tidal flooding, water encroaches on the landscape, where it can remain for hours, before returning to estuarine and coastal waters carrying nutrients and particles (Macias-Tapia et al. 2021 and 2023). Although critical progress has been made to reduce point- and nonpoint sources of nutrients in coastal areas (Sabo et al. 2022), tidal flooding is not currently included in the models used to design restoration strategies. Material (e.g., sediment, nutrients, and contaminating bacteria) transported into local and regional waterways as floodwaters recede after tidally driven flooding events are not routinely quantified. Ignoring inputs from tidal flooding, due to challenges in quantifying these loads, will impede restoration and preservation projects in coastal waterways (Macias-Tapia et al. 2021 and 2023).

Biotic and abiotic factors can influence the quality and quantity of nutrient inputs during tidal flooding. Rainfall prior to tidal flooding can saturate the ground and influence the magnitude of the floodwater volume (Xu et al. 2014; van den Hurk et al. 2015; Joyce et al. 2018). In the lower Chesapeake Bay, sustained winds from the north/northeast result in Ekman transport that drives higher than normal tides and enhanced tidal flooding (Shen and Gong 2009). Storms and high winds also result in sediment resuspension in this shallow estuarine system, which can enhance the flux of porewater nutrients to the water column (Kanoshinaa et al. 2003; Kalnejais et al. 2010). The amount of time flood water inundates the landscape, and the spatial extent of flooding varies by flooding event as well (Ezer 2018) and likely impacts nutrient loading (Macis-Tapia et al. 2021 and 2023). The heterogeneity of the land use (e.g., grass vs concrete) could also result in differences in the types of materials transported during the retreat of the flood tide thereby affecting estuarine water quality (Tu 2011). Studies have also shown that demographic changes, namely, increases in population and economic growth, are associated with decreases in water quality in natural water bodies (Juma et al. 2014; Liyanage and Yamada 2017).

Previous studies demonstrated that the nutrient loading associated with tidal flooding during perigean spring tides (i.e., king tides) between 2017 and 2021 was substantial but highly variable (Macias-Tapia 2021, 2023). These studies did not find clear correlations between nutrient loads due to tidal flooding and land use patterns. To better understand variability in nutrient loading due to tidal flooding, we established seven sentinel sites that experience frequent tidal flooding and sampled them over 15 tidal flooding events between January 2019 and September 2020, during major tidal flooding events. This allowed us to compare tidal flooding events over diverse meteorological conditions and seasonally varying biotic and abiotic factors that could influence nutrient loading from tidal flooding to the estuary. The initial hypothesis for the present study was that land use and meteorological conditions surrounding periods of tidal flooding play a major role in the quantity and quality of dissolved nutrient loads delivered to adjacent waters as tidewaters recede. The overarching goal of this study was to build a statistical model to predict nutrient loading to adjacent water bodies resulting from tidal flooding events. Such a model will allow us to estimate nutrient loading from tidal flooding during previous and future flooding events, and to adapt nutrient reduction strategies aimed at restoring aquatic ecosystems.

Methods

Study Area—Lafayette River

The study area was the Lafayette River watershed, an estuary located within the city of Norfolk, VA, at the southern end of the Chesapeake Bay (Fig. 1). The site receives fresh water from runoff and groundwater, has a temperate climate, and is a micro-tidal estuary with semi-diurnal tides (Sisson 1976). Most of the land that is located along the perimeter of the Lafayette River is prone to flooding because elevations are less than 5 m above mean sea level (Fig. S1A) (Kleinosky et al. 2007). Moreover, tidal flooding is predicted to

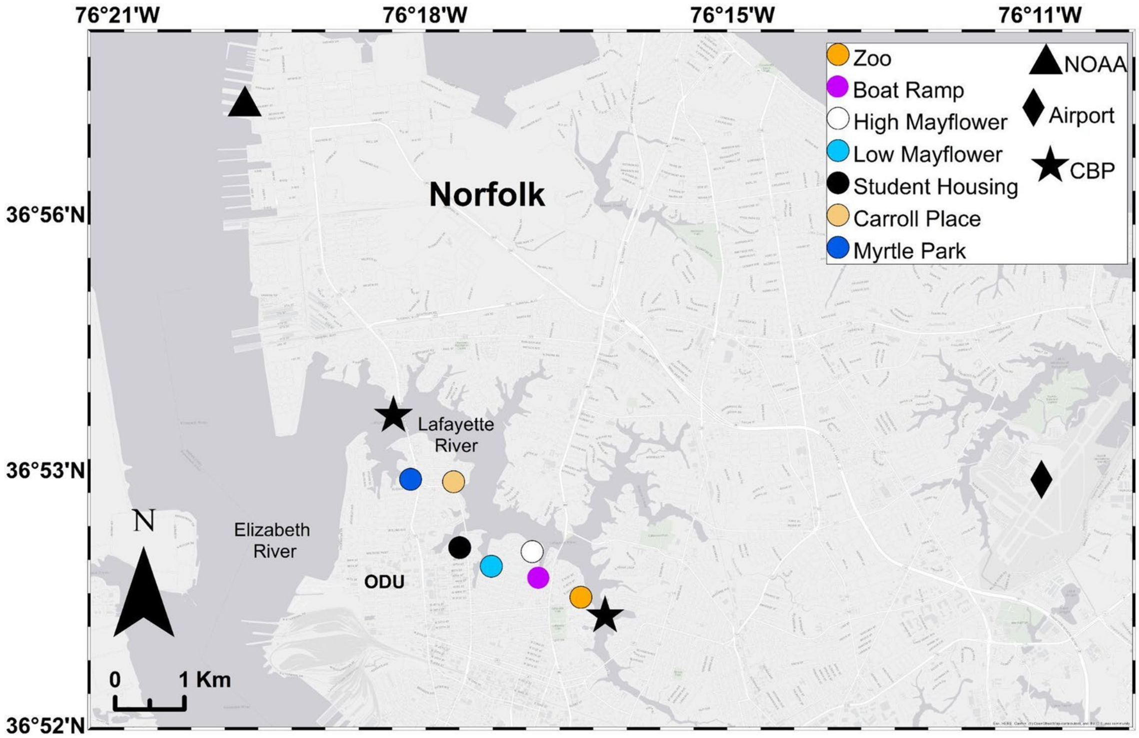

Fig. 1 Map showing sentinel sites (circles) where floodwater samples were collected during multiple tidal flooding events in 2019 and 2020. Stars represent the Chesapeake Bay Program (CBP) sites from which we extracted baseline dissolved nutrient concentrations. The triangle represents the NOAA meteorological station where water level and temperature data were collected. The rhombus represents the weather station at Norfolk International Airport from where precipitation and wind data were extracted

increase in frequency and intensity in the future (Fig. S1B) (Ezer 2018). The extent of the inundation in this region can be exacerbated by other factors like changes in the Gulf Stream and the occurrence of storms (e.g., Nor'easters) during spring tides (Ezer et al. 2013; Ezer and Atkinson 2014). According to the US Census Bureau, 235,089 people were living in Norfolk in 2021, with the median income around $50,000 (Fig. S1C). The Lafayette River watershed area is predominantly residential (68.99%); dump pits (i.e., roads or building construction) are the second most common land use type (5.60%) (Fig. S1D). Tree coverage (19.22%), turfgrass (14.18%), and impervious surfaces (12.38%) dominate the land cover along the perimeter of the estuary, with the percentage of wetlands (5.61%) increasing from the mouth to the head of the system (Fig. S1E). Landmarks located in the areas affected by flooding in Norfolk include the largest naval base in the USA and the Virginia Zoo (Spanger-Siegfried et al. 2014). Current precipitation estimates indicate that there are about 150 days of rain in any given year for this region, with annual precipitation of about 500 mm (https://www.weather-us.com). According to the 2021 Virginia Coastal Resilience Master Plan (https://www.dcr.virginia.gov), the region is experiencing more intense and frequent rainfall events when compared with long-term data. The windiest months are March and April, with an average peak wind speed of ~ 16 km h^{-1}, while the lowest average peak wind speeds (~ 12 km h^{-1}) occur in summer (Piecuch et al. 2016). Long-term monitoring by the Chesapeake Bay Program (CBP) shows average water temperatures in the Lafayette River ranging from ~ 5 °C in January to ~ 30 °C in July and average salinity values of ~ 19 in January and ~ 21 in July (https://data.chesapeakebay.net/WaterQuality).

Floodwater Samples

We measured dissolved nutrient concentrations in retreating floodwater at seven sentinel sites during 15 tidal flooding events occurring in all seasons between January 2019 to September 2020 (Fig. 1). Although most of the sites were residential or institutional, the sentinel sites had differences in their soil type and land use (Table S1). From the mouth of the estuary to the head, "Myrtle Park" site was the most residential area with a combination of pavement and turfgrass and a buffer wetland area planted at the edge of the water. "Carroll Place" is also residential, but a significant fraction of the flooded area is a park with a bulkhead located at the water's edge. The "Student Housing" site was in a residential area, but it has little grass and most of the area that floods is pavement. This sentinel site commonly had opened trash cans and trash littering the landscape. "Low Mayflower" is a residential area with similar proportions of pavement and turfgrass; this site was located near a commercial strip with restaurants and a marina. "High Mayflower" was similar to the "Low Mayflower" site but without businesses. "Boat Ramp" was a public boat launch with adjacent parking located in a residential area. This site sports a high concentration of paved surfaces, people deploying and recovering boats, and an adjacent dog park that frequently floods. "Zoo" was located at the downriver edge of the Virginia Zoo on a street with houses on one side and the Zoo on the other. The edge of the water has recently planted wetlands, while the rest of the area affected by tidal flooding is primarily pavement and soil with little planted grass.

To plan for sampling excursions, we monitored the National Oceanic and Atmospheric Administration (NOAA) tide and storm surge prediction website (https://tidesandcurrents.noaa.gov) to determine when water height was expected to be above that of the highest astronomically predicted high tide. During each sampling event, personnel drove to the sentinel sites at the peak of the high tide. At each site, we collected unfiltered floodwater in 250 mL Nalgene™ polycarbonate bottles (acid-cleaned, 10% HCl for 1 + days) near storm draining points. Bottles were rinsed three times with floodwater before sample collection. Three discrete samples were collected from each site to calculate an average and standard deviation (SD) for all measured quantities. Sample bottles were placed in a cooler with ice packs and kept in the dark until all sampling was complete (less than 1 h) and then transported to a laboratory at Old Dominion University (ODU) for processing.

At the laboratory, samples were filtered using combusted (450 °C for 4 h) Whatman GF75 glass fiber filters (pore size ~ 0.3 µm), and the filtrate was frozen until analysis. These samples were thawed before analysis of dissolved inorganic nitrogen (DIN) and dissolved inorganic phosphorus (DIP). Ammonium (NH_4^+) concentrations were quantified using the phenol hypochlorite method (Solorzano 1969) and a UV–Vis spectrophotometer (Shimadzu RF-1501). Nitrate plus nitrite (N + N) and DIP concentrations were measured using an Astoria Pacific Nutrient Autoanalyzer following the manufacturer's specifications for the standard colorimetric techniques of each analyte (Hansen and Koroleff., 1999). To calculate DIN, we summed the ammonium (NH_4^+) and N + N concentrations in each floodwater sample. The detection limit (DL) for each analyte was calculated using the SD of the lowest concentration used to construct the standard curve multiplied by three (3 × SD). Results below the limit of detection are reported as the detection limit. For each method, ultrapure water was analyzed in the same way as the samples to determine the value of the reagent blank.

Data Analysis

Differences Between Floodwater and Estuarine Concentrations

For the estuarine concentrations, we used data available from the CBP (https://data.chesapeakebay.net/WaterQuality) at two sites, at the head and mouth of the Lafayette River (Fig. 1). Specifically, we used surface (< 1 m) data collected on dates before each sampling at the sentinel sites. With the available values in both sites, we calculated an average to represent the conditions of dissolved nutrients on the surface waters of the system. Given the extensive variability in dissolved nutrient concentrations in floodwater samples collected during annual watershed-wide field campaigns between 2017 and 2021 (Macias-Tapia et al. 2021, 2023), outliers were removed before performing further data analysis. Upper and lower outliers were defined as values 1.5 times above the third quartile or below the first quartile, respectively. After removing the outliers, we calculated the difference in dissolved nutrient concentrations between floodwater and concentrations measured in the estuary prior to tidal flooding (ΔDIN and ΔDIP) for each sentinel site and flooding event.

Environmental and Demographic Data

Data to evaluate the relationship between floodwater nutrient concentrations and biotic/abiotic variables was extracted from different sources. Daily values of accumulated precipitation, and daily averages of wind speed and direction were collected from the Norfolk International Airport meteorological station (Fig. 1), whose data is publicly available (https://www.ncdc.noaa.gov). For precipitation, we calculated accumulated precipitation for the day of the sampling event and 3 days prior; for wind speed and direction, we used values from the day on which the sentinel site samples were collected. Maximum water temperatures and water levels were extracted from NOAA's meteorological station at Sewells Point (https://tidesandcurrents.noaa.gov/waterlevels.html?id=8638610), which is located near the mouth of the Lafayette River (Fig. 1). For our analysis, we used values of water temperature and water level from the same date in which floodwater samples were collected at the sentinel sites. Water level data is available using different reference points; here, we used the mean higher high water (MHHW) tidal datum, which positive values are associated with land inundated during tidal flooding events. For median income and total population, we used the 2019 U.S. Census Bureau data (https://data.census.gov/). Land use data was extracted from the Soil Survey Geographic database (SSURGO, https://data.nal.usda.gov/), while land cover data was obtained via the Virginia Geographic Information

Network (VGIN, https://vgin.vdem.virginia.gov/). As stated by the United States Department of Agriculture, the difference between land use and land cover is that the former involves elements of human activities, while land cover refers to physico-chemical properties specific to a given substrate (Nickerson et al. 2015). Land elevation was obtained from the US Geological Survey's National Elevation Dataset (USGS NED, https://www.sciencebase.gov). Using ArcMAP™, we performed a spatial join between the sentinel sites and potential control parameters (i.e., demographic, land use, land coverage, and elevation data) of the sentinel sites to extract the characteristics at the sampling locations.

Multi-Variable Random Forest Regression Model

Linear regression analyzes were performed between either ΔDIN or ΔDIP concentrations and a continuous variable. Before conducting linear regression analysis, we used the Kolmogorov–Smirnov test to check that the variables fit a normal distribution. For continuous variables, "Floodwater" is the concentration of DIN or DIP in floodwater, "Baseline" is the DIP or DIN concentration in the estuary prior to flooding, "1Rain" is the rainfall accumulation from the 24-h period prior to sampling, "3Rain" is the total accumulated precipitation for 3 days prior to the flooding event, "WindDir" and "WindSpd" are the average wind direction and speed the day of the flooding event, "WTemp" and "MHHW" are the maximum temperature and water level recorded the day of the flooding event, "Income" and "Population" are the median income per household and the total number of individuals in the area in which the floodwater sample was collected, and "Elevation" and "Slope" are the land elevation and slope steepness at the sites floodwater samples were collected. To perform the linear regression analysis and calculate its significance, we used the "linregress" function available within the SciPy Python library (Virtanen et al. 2020). We calculated the coefficient of determination (R^2) value and the p-value (p) and plotted the regression line when $p < 0.05$. To determine significant differences among sites, we used the non-parametric signed-rank. Differences were considered significant when $p < 0.05$.

Using the two variables with the highest R^2 values for the linear regression with either ΔDIN or ΔDIP, we built multi-variable random forest regression models. For all different combinations of variables, a total of 121 measurements were split into "training" (60%, $n = 73$) and "testing" (40%, $n = 48$) datasets. Grid Search cross-validation was performed on the fraction of training data to get the range of model accuracy using 2 to 40 "tree counts," 2 to 40 "maximum depth," and 10 "splits." "GridSearchCV" was used to assess the best combination of parameters. The results from the Grid Search were used to build the best possible model for ΔDIN and ΔDIP, respectively. Using the testing dataset, a linear regression model of the predicted versus the measured ΔDIN and ΔDIP was run to evaluate the performance of the multi-variable random forest regression model. This procedure was repeated 70 times for each multi-variable random forest regression model. For each repetition, the "training" and "testing" split was performed on the original dataset. The average and standard deviation were calculated for each model.

Prior to this study and those of Macias-Tapia et al. (2021 and 2023), biochemical characterization of tidal flooding has been limited. Thus, we built models without dissolved nutrient concentrations in floodwater as a predictor variable to allow us to calculate loads of dissolved inorganic N and P during flooding events for which floodwater nutrient concentrations are not available. The same tree counts, maximum depth, and splits were used to build these models, and the results were also tested by comparing predicted and measured values.

The temporal availability of data used in the multi-variable random forest regression models varied among the three predicting variables (Fig. S11 A-D). Water level and temperature were available hourly from the Sewells Point NOAA meteorological station. Water level data was available from 1930 to present, while records of water temperature are available since 1996 (Fig. S11 A-B). Daily wind data was available from 1984 to present at Norfolk International Airport weather station (Fig. S11 C).

Nutrient Inputs During Tidal Flooding Events

To calculate loads of dissolved nutrients delivered during previous tidal flooding events, we multiplied the inundation volume for each event by predicted ΔDIN and ΔDIP. To determine inundation volume, we calculated floodwater volumes for each event based on the MHHW data available from the NOAA meteorological station located near the mouth of the Lafayette River (Fig. 1) and the relationship between the floodwater volume and MHHW during five perigean spring tides between 2017 and 2021 (Macias-Tapia et al. 2023) (Fig. S2). For the ΔDIN and ΔDIP values, we used the best-performing multi-variable random forest regression models, when dissolved nutrient concentrations in floodwater were and were not available. To calculate net fluxes, we added the values (both positive and negative) calculated during single tidal flooding events. The sum of values extended temporarily as far as single nutrient flux estimations were available.

Results

We collected 190 floodwater samples from sentinel sites during 15 tidal flooding events between January 2019 and September 2020 (Table 1). Not all sentinel sites were sampled during each incidence of tidal flooding due to differences in the extent of the tidal flooding in each event and the land elevation at each sampling site. Also, more tidal flooding events occurred during the time-period of this study, but personnel were not always available to collect samples.

Among the floodwater samples collected, median DIN concentrations over the entire length of the study ranged from 3.9 μM at Carroll Place to 10.6 μM at the Zoo sampling sites (Table 1). For DIP, median concentrations ranged from 3.15 μM at the Zoo, to 7.88 μM at Myrtle Park. Only the Myrtle Park sentinel site had maximum values beyond the outlier threshold established for both DIN and DIP. The outlier concentrations were 178 and 49.1 μM of DIN and DIP, respectively. The day those samples were collected, there was colored water bubbling up from one of the drainage systems nearby (Fig. S3). Those values were removed before continuing with the remaining steps to build the model to predict nutrient loads during tidal flooding events.

Values for ΔDIN and ΔDIP were similar among sentinel sites (Fig. 2). The ΔDIN ranged from > -20 to < 30 μM (Fig. 2A); results from the non-parametric signed-rank tests indicate that values from the Carroll Place and Student Housing sentinel sites were statistically lower than those from the High Mayflower, Boat Ramp, and Zoo. For ΔDIP, values ranged from > -5 to 25 μM, with only the Myrtle Park and Zoo sites showing statistically significant differences from each other (Fig. 2B).

Relationship with Environmental and Demographic Variables

The slope and R^2 value of the linear regressions between either ΔDIN and ΔDIP, and the various environmental and demographic data varied depending on the parameters compared (Table 2). The concentration of dissolved nutrients in floodwater had high correlation values with both ΔDIN ($R^2 = 0.73$) and ΔDIP ($R^2 = 0.99$). DIN concentrations in floodwaters ranged from the analytical DL to nearly 40 μM, while DIP concentrations ranged from DL to ~ 25 μM (Fig. S4 A-B). DIN estuarine concentrations in baseline samples ranged from DL to nearly 20 μM, while estuarine DIP concentrations ranged from DL to about 2.0 μM (Fig. S4 C-D). R^2 values were 0.05 for DIN and 0.01 for DIP (Table 2). Precipitation ranged from 0 to 91.4 mm for the specific dates on which samples were collected, while accumulated rain three days before sampling ranged from 0 to 134.6 mm (Fig. S5). The linear regressions between precipitation and ΔDIP or ΔDIN were not statistically significant (Table 2). For most of the sampling events at the sentinel sites, the wind direction was between 0 and 200 degrees (e.g., generally from the east; Fig. S6 A-B). There was no correlation between wind direction and either ΔDIN or ΔDIP (Table 2). Wind speed ranged from 5.8 to 35.2 km h^{-1} (Fig. S6 C-D). For ΔDIN, there was a significant correlation with wind speed ($R^2 = 0.11$, $p = 1.13 \times 10^{-5}$). The correlation between ΔDIP and wind speed was also significant ($p = 1.4 \times 10^{-10}$) and had a higher R^2 ($R^2 = 0.15$). Water temperature at the mouth of the Lafayette River varied throughout the year from 5.2 to 28.2 °C (Fig. S7). Both ΔDIN and ΔDIP had significant albeit weak correlations with water temperature ($R^2 = 0.25$ for ΔDIN and $R^2 = 0.18$ for ΔDIP; Table 2). The extent of flooding during the sampling campaigns at the sentinel sites ranged from 0.1 to 0.5 m above MHHW (Fig. S8). Both ΔDIN and ΔDIP had significant linear regressions with MHHW but differed in the R^2 values (0.19 and 0.08, respectively; Table 2). The median income at the regions in which the sentinel sites were located ranged from < 20,000 to 100,000 $US (Fig. S9 A-B). The total population for the same regions ranged from 2000 to 5000 individuals (Fig. S9 C-D). Income and population had low R^2 values for both ΔDIP or ΔDIN (Table 2).

In terms of land use, Carroll Place, Boat Ramp, Myrtle Park, and High Mayflower sampling sites fell under "Dump pit" SSURGO characterization, which refers to areas of smoothed or uneven accumulations of general refuse; Zoo fell under "Bohicket muck," which are poorly drained, slowly permeable soils that formed in marine sediments in tidal marshes; and the Student Housing and Low Mayflower sites were characterized as "Urban Complex," which is dominated by impermeable surfaces like buildings and pavement. Values of both ΔDIN and ΔDIP were statistically similar among SSURGO land use categories (Fig. 3A, B). Following VGIN land cover data, Carroll Place, Boat Ramp, Low Mayflower, Myrtle Park, and Student Housing all were characterized as "impervious," which refers to areas characterized by a high percentage of constructed materials (e.g., asphalt and concrete); High Mayflower was characterized as "turfgrass," which primarily includes grasses and herbaceous vegetation, planted and naturally occurring; and the Zoo site fell under "wetlands," which includes fully formed and emergent vegetation in areas of land saturated with

Table 1 The number of samples at each sentinel site (*n*), median, and maximum concentrations of DIN (μM) and DIP (μM) in floodwater samples collected at the sentinel sites during multiple flooding events. Maximum values marked with an asterisk (*) indicate outliers

		DIN		DIP	
Sampling site	*n*	Median	Max	Median	Max
Myrtle Park	52	5.73	177.67*	7.88	49.05*
Carroll Place	38	3.91	16.92	3.56	16.08
Student Housing	18	4.70	20.39	5.45	10.89
Low Mayflower	20	7.31	28.44	3.68	23.72
High Mayflower	21	8.73	25.85	7.64	20.48
Boat Ramp	29	6.86	23.11	7.09	14.20
Zoo	12	10.59	30.95	3.15	21.42

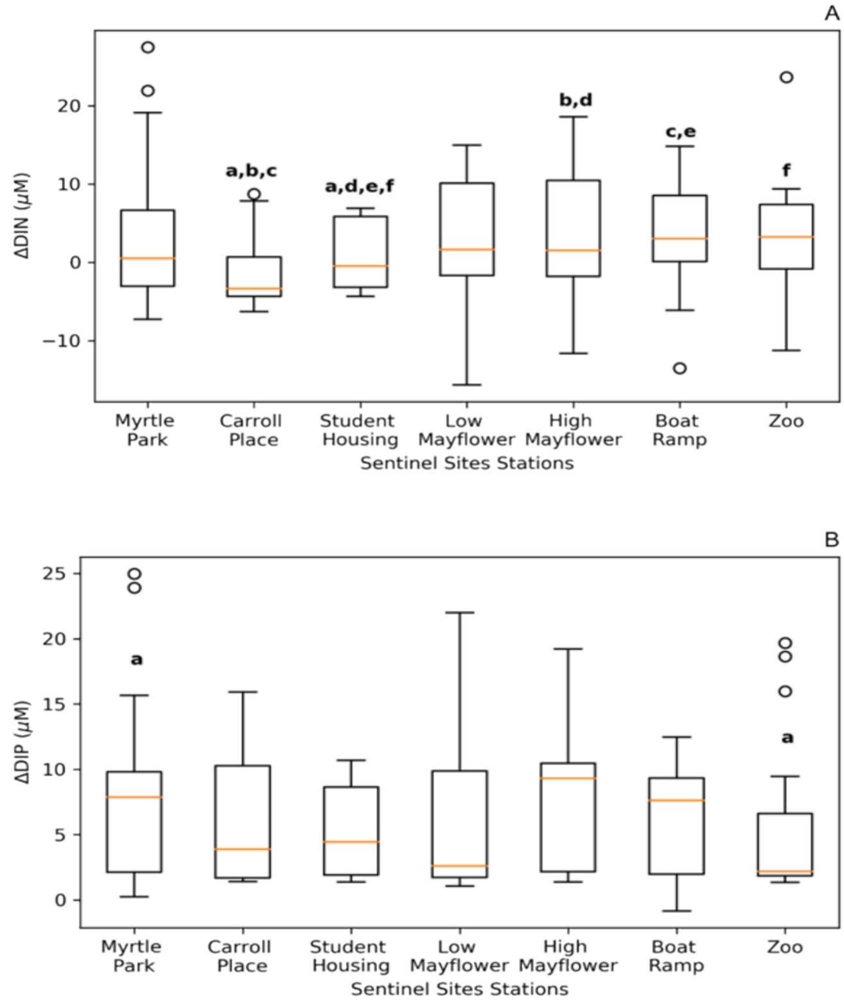

Fig. 2 Box and whisker plot of **A** ΔDIN and **B** ΔDIP at the different sentinel sites. The lowercase letters on top of each box indicate that ΔDIN and ΔDIP values at those sites are statistically different (Table S2). The orange line and the whiskers in each box represent the median and the SD of each group, respectively

water. There was no statistical difference between ΔDIN or ΔDIP and the different VGIN land cover categories (Fig. 3C, D).

Multi-variable Random Forest Regression Model

Model with Dissolved Nutrient Concentrations in Floodwater Available

For ΔDIN, R^2 values for the different versions of the random forest regression models ranged from 0.65 to 0.94 (Table 3, A). The model with the highest performance ($R^2 = 0.94 \pm 0.01$) was the one in which all the available variables were included (i.e., Flood, MHHW, and WTemp. See Table 2 for abbreviations), followed closely by the models that included floodwater DIN concentrations and either water temperature or water level data. The model with the lowest performance was the one that only used floodwater DIN as the predictor variable ($R^2 = 0.65 \pm 0.08$). For DIP, all the models had $R^2 > 0.98$ (Table 3, B).

Using the best performing models for each nutrient, predicted ΔDIN ranged from − 15 to 15 μM, with slight differences among models (Fig. S10 A), while predicted ΔDIP had virtually the same values for all models and ranged between 2 and 14 μM (Fig. S10 B). Inundation volumes during the different sampling events at the sentinel sites ranged from about 3 to 5.5×10^7 m^3 (Fig. S10C). Using the estimated ΔDIP or ΔDIN, with the inundation volumes during each sentinel site sampling, we calculated the nutrient loads delivered during each flooding event (Fig. 4). Based on these calculations, the DIN flux per event ranged from − 5000 to 7500 kg N (Fig. 4A), while Net DIN load went from − 5000 to > 5000 kg N. For DIP, the estimated flux in a single tidal flooding event ranged from 2000 to 23,000 kg P (Fig. 4B), while Net DIP load steadily accumulated to > 100,000 kg P.

Model Without Floodwater Dissolved Nutrient Concentration Data

When nutrient concentrations in floodwaters were not included, the capabilities of different multi-variable

Table 2 R^2 and *p*-values (*p*) for each estimated linear regression between ΔDIP or ΔDIN (in μM) and environmental and demographic variables. Significant correlations are highlighted with **bold** font. "Floodwater" is the concentration of DIN or DIP in floodwater, "Baseline" is the DIP or DIN concentration in the estuary prior to flooding, "1Rain" is the rainfall accumulation from the 24-h period prior to sampling, "3Rain" is the total accumulated precipitation for 3 days prior to the flooding event, "WindDir" and "WindSpd" are the average wind direction and speed the day of the flooding event, "WTemp" and "MHHW" are the maximum temperature and water level recorded the day of the flooding event, "Income" and "Population" are the median income per household and the total number of individuals in the area in which the floodwater sample was collected, and "Elevation" and "Slope" are the land elevation and slope steepness at the sites floodwater samples were collected

	ΔDIN		ΔDIP	
Variable	R^2	*p*	R^2	*p*
Flood	0.73	4.7×10^{-49}	0.99	3.7×10^{-228}
Baseline	0.05	2.3×10^{-3}	0.01	1.4×10^{-1}
WTemp	0.25	5.9×10^{-12}	0.18	2.8×10^{-12}
MHHW	0.19	5.6×10^{-9}	0.08	3.6×10^{-6}
WindSpd	0.11	1.1×10^{-5}	0.15	1.4×10^{-10}
WindDir	0.01	2.3×10^{-1}	0.01	2.6×10^{-1}
1Rain	0.01	3.1×10^{-1}	0.0	6.9×10^{-1}
3Rain	0.00	3.8×10^{-1}	0.0	4.8×10^{-1}
Population	0.01	1.2×10^{-1}	0.0	8.1×10^{-1}
Income	0.0	7.8×10^{-1}	0.0	5.8×10^{-1}
Elevation	0.0	5.0×10^{-1}	0.0	3.9×10^{-1}
Slope	0.0	5.6×10^{-1}	0.0	8.0×10^{-1}

random forest regression models to predict N and P loading dropped (Table 4, A and B). For each nutrient, only the two parameters with the highest R^2 values were used in the model (Table 2). For ΔDIN, the best-performing model was the one using MHHW ($R^2 = 0.71 \pm 0.04$) as the only predictor variable followed by the model combining MHHW and WTemp as predictor variables ($R^2 = 0.70 \pm 0.02$) (Table 4, A). The model using WTemp as the only predictor variable showed the lowest performance ($R^2 = 0.67 \pm 0.09$). For ΔDIP, the models with WindSpd and WTemp or just WTemp had $R^2 \geq 0.70$, while the model with WindSpd alone had an $R^2 = 0.41$ (Table 4, B).

Predicted ΔDIN varied between the two models considered (i.e., MHHW and MHHW + WTemp) (Fig. S12A). Values for ΔDIN ranged between ~ 0 and 12 μM when using MHHW as the only predictor variable, while ΔDIN values ranged between ~ 4 and ~ 9 μM when adding WTemp as a predictor variable. Because of the differences in temporal availability of the data informing the models, ΔDIN predicted values using the MHHW model are available from 1950, while results from the MHHW + WTemp model are only available from 1996. Results for predicted ΔDIP were similar for the two models considered (i.e., WTemp and WTemp + WindSpd) (Fig. S12B), with values ranging from − 3 to 3 μM.

Predicted ΔDIP was lower than 15 μM for the WTemp and WTemp + WindSpd models, but the WTemp + WindSpd model predicted ΔDIP as low as − 15 μM (Fig. S12B). Both ΔDIP models show results from 1996 because of the availability restrictions on the WTemp data. Water levels measured during the maximum tidal-driven flooding event near the mouth of the study area each year since 1946 ranged from > 0 to < 1 m (Fig S13). Estimated inundation volumes calculated using the relationship between MHHW and inundation volume observations (Fig. S2) ranged from 5×10^7 to 9×10^7 m^3 (Fig. S13).

Predicted loads of dissolved inorganic N and P (i.e., DIN and DIP, respectively) during past tidal-driven flooding events changed depending on the model used, but it was overall positive and had an increasing trend over time (Fig. 5A, B). Predicted DIN load estimates were the highest when using the MHHW model, ranging from ~ 0 to 1.5×10^5 kg (Fig. 5A), and showed a significant linear regression from 1950 to 1990 ($R^2 = 0.2$ and $p = 2 \times 10^{-4}$) and a steeper for data after 1990 ($R^2 = 0.7$ and $p = 7 \times 10^{-10}$). The MHHW + WTemp model estimates of net nutrient load ranged from -2.5×10^4 kg to 1.0×10^5 kg and also had statistically significant linear regressions with time ($R^2 = 0.6$ and $p = 2 \times 10^{-6}$). Predicted DIP load estimates during past tidal-driven flooding events were similar for the two models and ranged from -1.0×10^5 to 1.5×10^5 kg (Fig. 5B). Results for both models showed a significant positive trend of net DIP loads over time and had similar R^2 (0.3) and p (1×10^{-4}).

Discussion

Tidal Flooding Events as a Source of Dissolved Nutrients

Five years of spatially extensive sampling during annual king tides revealed that tidal flooding events convey terrestrial nutrients to adjacent waters (Macias-Tapia et al. 2021, 2023). While the earlier studies were spatially extensive, they focused on singular perigean spring tide events each year (Macias-Tapia et al. 2023). To evaluate the effects of seasonality and antecedent meteorological conditions on the magnitude of nutrient loading during tidal flooding, more frequent floodwater sample collection was needed. Here, we present results from a sampling approach that included seven sampling sites, sampled fifteen times over the course of four seasons and 2 years. These sampling campaigns included diverse meteorological and biotic conditions that enabled us to build a statistical model to predict DIN and DIP loads from tidal flooding (Figs. 4 and 5), work that is essential for advising estuarine restoration as sea levels continue to rise.

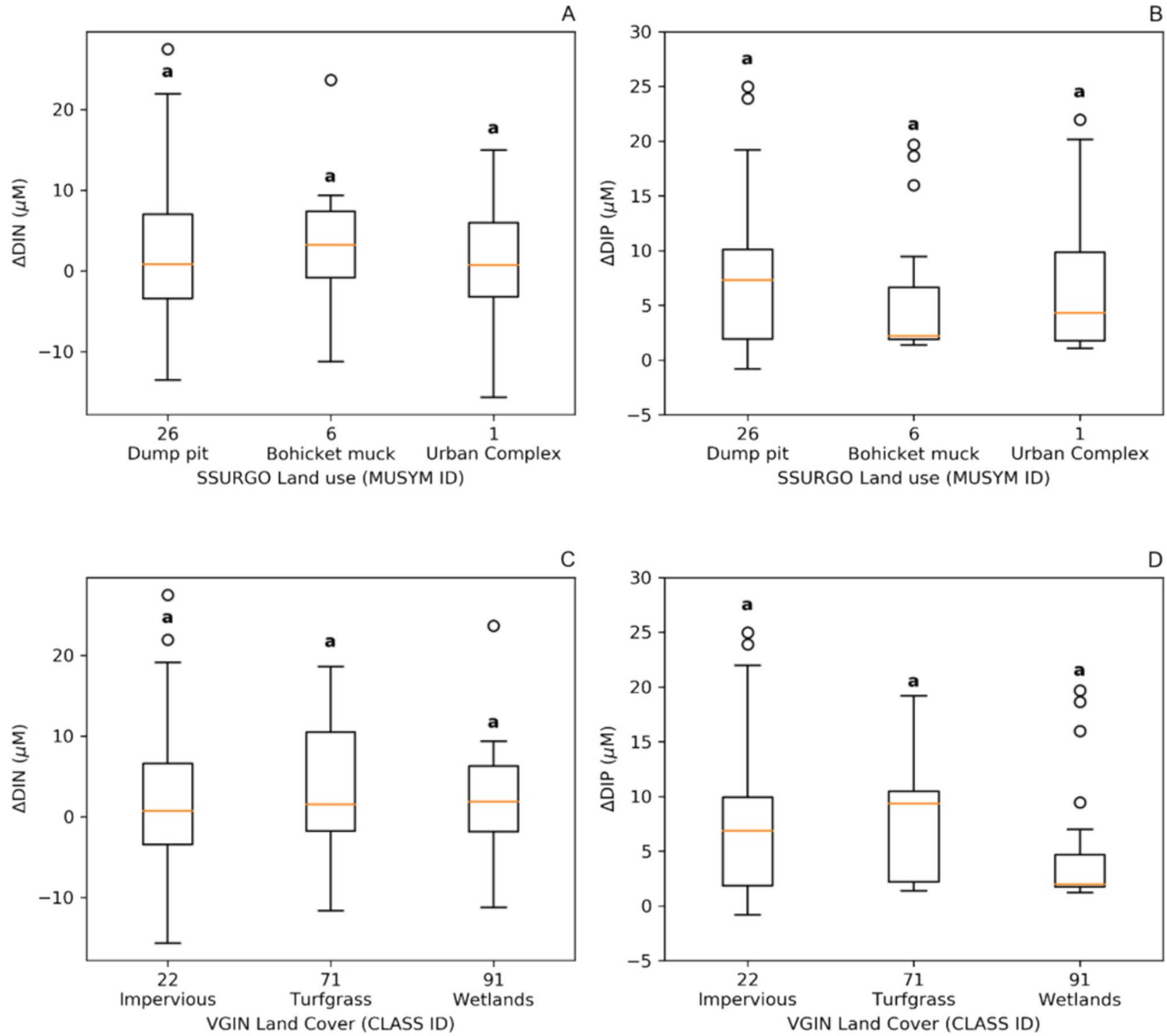

Fig. 3 Relationships between ΔDIP or ΔDIN (both in μM) and SSURGO land use types **A**, **B** and VGIN designated land coverage **C**, **D**. Panels on the left are for ΔDIN, while panels on the right are for ΔDIP. The orange line and the whiskers in each box represent the median and the SD of each group, respectively. The lowercase letters on top of each box indicate values that were statistically similar among land use or cover categories

The models in which floodwater nutrient concentrations were used as a predictor variable had high performance ($R^2 > 0.9$) estimating ΔDIN and ΔDIP values. However, there is a lack of data on dissolved nutrient concentrations (including N and P) in floodwaters during tidal flooding events. Thus, we also built models without associated floodwater nutrient concentration data. Models built with and without dissolved nutrient concentrations in floodwater predicted positive net loads over time and, in all cases, loading estimates exceeded annual load allocations established by the U.S. Environmental Protection Agency (EPA) for the Lafayette River. These values are known as Total Maximum Daily Loads (TMDLs) allocations, which were established in 2010 to restore the water quality of the Chesapeake Bay and its tributaries (Wainger 2012). These results are alarming because this load is not included in any existing TMDL, while the occurrence of this transportation of dissolved nutrients is increasing due to sea level rise (Macias-Tapia et al. 2021, 2023).

Along with the general results of this study on fluxes of dissolved nutrients during tidal flooding events, we found a decoupling in the direction and magnitude of N and P loading estimates (Fig. 5). The magnitude and the trend for the DIN model differ more than those for DIP. The main driver

Table 3 R^2 results for measured versus predicted A) ΔDIN and B) ΔDIP values from the multi-variable random forest regression model built with combinations of the best predicting variables (from Table 2). Model repetitions are shown on the left and subsequent columns are model runs using different combinations of predicting variables (e.g., Flood/MHHW/WTemp, Flood/WTemp, Flood/MHHW, or Flood; see Table 2 for abbreviations). At the bottom of each column, we show the average R^2 value and SD for each model. Columns with values in bold letters represent the models with the highest R^2 results, which were used in the next step to calculate nutrient loads during flooding events

	A) ΔDIN				B) ΔDIP			
Repetition	Flood MHHW WTemp	Flood WTemp	Flood MHHW	Flood	Flood WindSpd WTemp	Flood WindSpd	Flood WTemp	Flood
10	0.96	0.94	0.93	0.52	0.98	0.99	0.99	0.99
20	0.92	0.97	0.88	0.72	0.99	0.99	0.99	0.99
30	0.96	0.77	0.90	0.70	0.99	0.99	0.99	0.99
40	0.95	0.96	0.91	0.59	0.98	0.99	0.99	0.99
50	0.93	0.96	0.93	0.71	0.99	0.99	0.99	0.99
60	0.97	0.96	0.93	0.58	0.99	0.99	0.99	0.99
70	0.95	0.94	0.91	0.75	0.99	0.99	0.99	0.99
Avg	0.94	0.92	0.91	0.65	0.98	0.99	0.99	0.99
SD	0.01	0.06	0.01	0.08	0.00	0.00	0.00	0.00

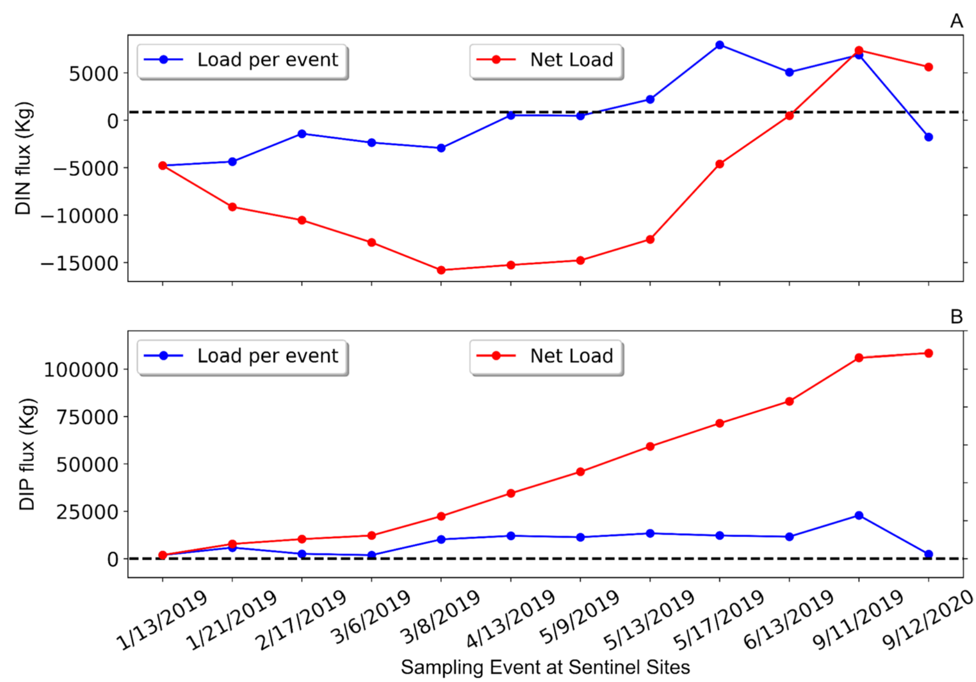

Fig. 4 Nutrient load per floodwater sampling event at the sentinel sites (in blue) and overall (in red) for DIN **A** and DIP **B**. The dotted line corresponds to the annual limit land-based allocation for total nitrogen (880 kg) and total phosphorus (58 kg) according to the EPA's TMDLs

Table 4 R^2 results from measured ΔDIN and ΔDIP versus values predicted using a multi-variable random forest regression model built with combinations of the best single environmental predictors when measurements of nutrient concentrations in floodwater are not available. Columns with values in bold letters represent the models with the highest R^2 results, which were used in the next step to calculate nutrient loads during flooding events

A) ΔDIN	MHHW			B) ΔDIP	WindSpd		
	WTemp	WTemp	MHHW		Wtemp	WindSpd	Wtemp
avg	0.70	0.67	0.71	avg	0.68	0.41	0.66
SD	0.02	0.09	0.04	SD	0.01	0.01	0.08

Fig. 5 Net Load represents the accumulated flux of **A** DIN and **B** DIP during tidal flooding events. Different colors represent the model used to predict the value. The name of the model represents the variables used to build the random forest regression model. The dashed line represents the fitting regression line when $p < 0.05$ for each model. R^2 and p for each linear regression are shown at the end of each line

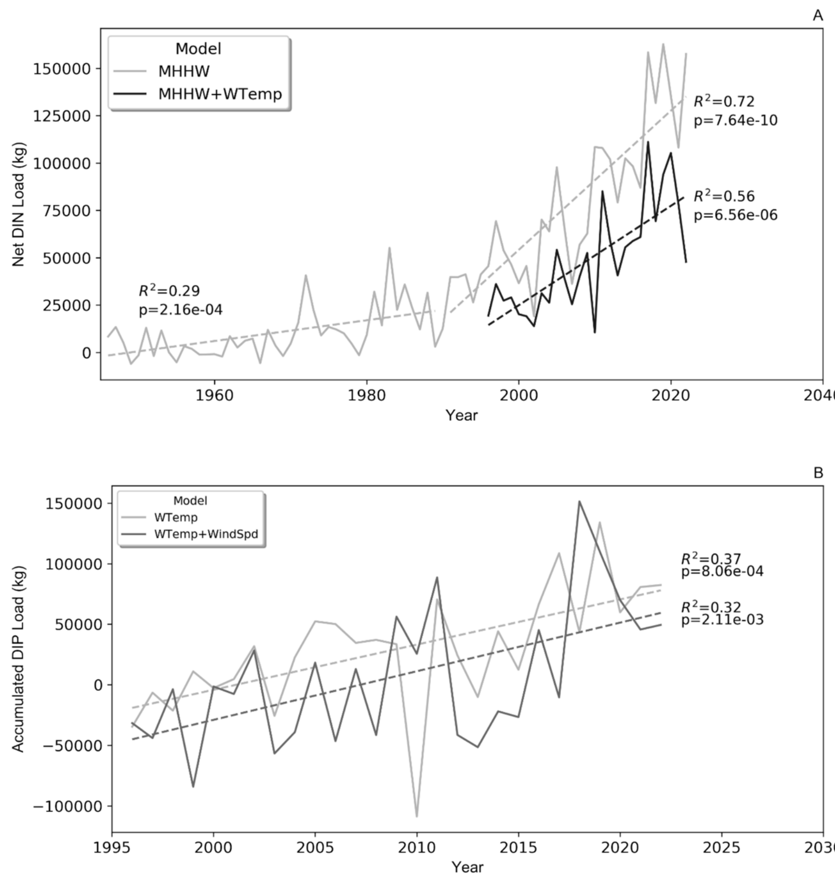

of this difference is the use of water level data to predict DIN but not DIP. These differences could affect the biological processes in receiving waters as primary productivity in more saline waters is typically N limited while fresh waters tend to be P limited (Howarth and Marino 2006).

Variables That Control Nutrient Loads During Tidal Flooding

Meteorological and hydrological variables, namely, the extent of high waters during the flooding event, water temperature, and wind speed were the best predictors of the magnitude of nutrient loads delivered from tidal flooding. Weather conditions have previously been recognized as playing a role in controlling nutrient loads during non-tidal-driven flooding events (Hale et al. 2015). Prior precipitation can remove materials from the landscape, thereby reducing nutrient loading from tidal flooding (Selbig 2016). In addition, the magnitude of tidal flooding determines the amount of time floodwaters interact with the landscape (Ezer 2018; Macias-Tapia et al. 2023). Wind speed and direction not only influence the magnitude of tidal flooding, but can cause materials to accumulate in specific areas (Pirazzoli 2000; Shen and Gong 2009). Further, water temperature controls the rates of nutrient transformations and exchanges in estuarine waters as these processes are mediated by resident bacteria and phytoplankton (Hallegraeff 2010; Marinov et al. 2010; Lewandowska et al. 2014).

Similar to a previous study, correlations between concentrations of dissolved nutrients delivered and land use/cover could not be discerned by this study (Macias-Tapia et al. 2023). In this study, neither land characteristics nor demographic data of the sampling sites correlated with the magnitude of inorganic nutrient loading during tidal flooding events. This may have been because the land elevation, total population, income, land use, and land cover values were too similar in the Lafayette River (Fig. S1 A-E), or that nutrient loads are integrated over aggregated regions within a watershed. Future studies should target catchments in which the differences in the values of these and other variables are more pronounced.

Nutrient Hot Spots During Tidal Flooding

Similar to Macias-Tapia et al. (2021 & 2023), we found that certain sites were hot spots for dissolved nutrient concentrations in floodwater with values orders of magnitude higher than the median of the samples collected at the sentinel sites over multiple flooding events. Hot spots appeared to coincide with drainage systems that backflow during high tides (Fig. S3). Tidal flooding in Norfolk can be initiated through stormwater drains at high tides, causing streets to flood as water rises through the drains, even if they are not adjacent to the river (Shen et al. 2019). These drains can be hot spots for microbial activity as residual water is retained in the storm sewer system where it can incubate (Aryal et al. 2021). Neither this nor previous studies conducted focused investigations at drainage sites. Better understanding of how storm drains act as microbial incubators could potentially increase estimates of nutrient inputs and microbial contamination from tidal flooding. A study that targets these areas should be carried out to better understand microbial-nutrient interactions at these hotspots. Because these storm drains are located at points within the tidal watershed, they could potentially be targets for remediation.

Conclusions

After a spatially extensive sampling of floodwater in an urban tributary of the lower Chesapeake Bay, we found the following: (1) ΔDIN showed the strongest correlations with water level and water temperature, while ΔDIP was most highly correlated with wind speed and water temperature. (2) The lack of correlation between floodwater DIN and DIP with land elevation, total population, income, land use, and land cover might be because values for these variables were similar for the areas affected by tidal flooding in the Lafayette River. (3) Multi-variable random forest regression models in which nutrient concentrations in floodwater were available had $R^2 > 0.9$, while models in which this variable was not used had $R^2 \approx 0.7$. This shows that although biochemical characterization of tidal flooding events allows us to closely understand the fluxes of DIN and DIP in coastal areas, models without this variable still showed good predicting capabilities and allowed us to analyze long-term data. (4) There was a positive trend in nutrient loads corresponding to water level, demonstrating that loads are increasing as sea level rises and tidal flooding becomes more common, resulting in the eutrophication of the region. The biochemical characterization of more coastal areas affected by tidal flooding events with different weather conditions, will allow to build better models, enabling more effective management and mitigation strategies.

Supplementary Information The online version contains supplementary material available at https://doi.org/10.1007/s12237-024-01473-1.

Acknowledgements The authors would like to thank the Hampton Roads Sanitation District (HRSD) and the Blocker Foundation for funding this project.

Declarations

Conflict of Interest The authors declare no competing interests.

References

Adu, J.T., and M.V. Kumarasamy. 2018. Assessing non-point source pollution models: a review. *Polish Journal of Environmental Studies* 27: 1913–1922. https://doi.org/10.15244/pjoes/76497.

Aryal, R., J.P.S. Sidhu, N.C. Meng, S. Toze, W. Gernjak, and B. Mainali. 2021. Role of environmental variables in the transport of microbes in stormwater. *Water* 13 (9): 1146. https://doi.org/10.3390/w13091146.

Berdalet, E., L.E. Fleming, R. Gowen, et al. 2016. Marine harmful algal blooms, human health and wellbeing: challenges and opportunities in the 21st century. *Journal of the Marine Biological Association of the United Kingdom.* 96 (1): 61–91. https://doi.org/10.1017/S0025315415001733.

Bouraoui, F., and B. Grizzetti. 2011. Long term change of nutrient concentrations of rivers discharging in European seas. *Science of The Total Environment* 409: 4899–4916. https://doi.org/10.1016/j.scitotenv.2011.08.015.

Brown, T.C., and P. Froemke. 2012. Nationwide assessment of non-point source threats to water quality. *BioScience* 62: 136–146. https://doi.org/10.1525/bio.2012.62.2.7.

Cabral, H., V. Fonseca, T. Sousa, and C.L. Miguel. 2019. Synergistic effects of climate change and marine pollution: an overlooked interaction in coastal and estuarine areas. *International Journal of Environmental Research and Public Health* 16: 2737. https://doi.org/10.3390/ijerph16152737.

Ezer, T. 2018. The increased risk of flooding in Hampton Roads: On the roles of sea level rise, storm surges, hurricanes, and the gulf stream. *Marine Technology Society Journal* 52: 34–44. https://doi.org/10.4031/MTSJ.52.2.6.

Ezer, T., and L.P. Atkinson. 2014. Accelerated flooding along the U.S. East coast: On the impact of sea-level rise, tides, storms, the Gulf Stream, and the North Atlantic Oscillations. *Earth's Future* 2: 362–382. https://doi.org/10.1002/2014EF000252.

Ezer, T., L.P. Atkinson, W.B. Corlett, and J.L. Blanco. 2013. Gulf Stream's induced sea level rise and variability along the US mid-Atlantic coast. *Journal of Geophysical Research: Oceans* 118: 685–697. https://doi.org/10.1002/jgrc.20091.

Hale, R.L., N.B. Grimm, C.J. Vorosmarty, and B. Fekete. 2015. Nitrogen and phosphorus fluxes from watersheds of the northeast U.S. from 1930 to 2000: Role of anthropogenic nutrient inputs, infrastructure, and runoff. *Global Biogeochemical Cycles* 29: 341–356. https://doi.org/10.1002/2014GB004909.

Hallegraeff, G. 2010. Ocean climate change, phytoplankton community responses, and harmful algal blooms: A formidable predictive challenge. *Journal of Phycology* 46: 220–235. https://doi.org/10.1111/j.1529-8817.2010.00815.x.

Hansen, H.P., and F. Koroleff. 1999. Determination of nutrients. In Methods of Seawater Analysis, eds K. Grasshoff, K. Kremling and M. Ehrhardt. WILEY. https://doi.org/10.1002/9783527613984.ch10.

Howarth, R.W., and R. Marino. 2006. Nitrogen as the limiting nutrient for eutrophication in coastal marine ecosystems: evolving views over three decades. *Limnology and oceanography* 51 (1part2): 364–376.

Joyce, J., N.B. Chang, R. Harji, T. Ruppert, and P. Singhofen. 2018. Cascade impact of hurricane movement, storm tidal surge, sea level rise and precipitation variability on flood assessment in a coastal urban watershed. *Climate Dynamics* 51: 383–409. https://doi.org/10.1007/s00382-017-3930-4.

Juma, D.W., H. Wang, and F. Li. 2014. Impacts of population growth and economic development on water quality of a lake: Case study of Lake Victoria Kenya water. *Environmental Science and Pollution Research* 21: 5737–5746. https://doi.org/10.1007/s11356-014-2524-5.

Kalnejais, L., W. Martin, and M. Bothner. 2010. The release of dissolved nutrients and metals from coastal sediments due to resuspension. *Marine Chemistry* 121: 224–235. https://doi.org/10.1016/j.marchem.2010.05.002.

Kanoshinaa, I., U. Lipsb, and J.M. Leppänen. 2003. The influence of weather conditions (temperature and wind) on cyanobacterial bloom development in the Gulf of Finland (Baltic Sea). *Harmful Algae* 2: 29–41. https://doi.org/10.1016/S1568-9883(02)00085-9.

Kleinosky, L.R., B. Yarnal, and A. Fisher. 2007. Vulnerability of Hampton Roads, Virginia to storm-surge flooding and sea-level rise. *Natural Hazards* 40: 43–70. https://doi.org/10.1007/s11069-006-0004-z.

Lewandowska, A.M., H. Hillebrand, K. Lengfellner, and U. Sommer. 2014. Temperature effects on phytoplankton diversity — the zooplankton link. *Journal of Sea Research* 85: 359–364. https://doi.org/10.1016/j.seares.2013.07.003.

Liyanage, C.P., and K. Yamada. 2017. Impact of population growth on the water quality of natural water bodies. *Sustainability* 9: 1405. https://doi.org/10.3390/su9081405.

Macías-Tapia, A., M.R. Mulholland, C.R. Selden, J.D. Loftis, and P.W. Bernhardt. 2021. Effects of tidal flooding on estuarine biogeochemistry: Quantifying flood-driven nitrogen inputs in an urban, lower Chesapeake Bay sub-tributary. *Water Research* 201: 117329. https://doi.org/10.1016/j.watres.2021.117329.

Macías-Tapia, A., M.R. Mulholland, C.R. Selden, J.D. Loftis, and P.W. Bernhardt. 2023. Five years measuring the muck: Evaluating interannual variability of nutrient loads from tidal flooding. *Estuaries and Coasts* 46: 1756–1776. https://doi.org/10.1007/s12237-023-01245-3.

Malone, T.C., and A. Newton. 2020. The globalization of cultural eutrophication in the coastal ocean: causes and consequences. *Frontiers in Marine Science* 7: 2296–7745. https://doi.org/10.3389/fmars.2020.00670.

Marinov, I., S.C. Doney, and I.D. Lima. 2010. Response of ocean phytoplankton community structure to climate change over the 21st century: partitioning the effects of nutrients, temperature and light. Biogeosciences 7:3941–3959. https://doi.org/10.5194/bg-7-3941-2010

Nicholls, R., and A. Cazenave. 2010. Sea-level rise and its impact on coastal zones. *Science* 328: 1517–1520. https://doi.org/10.1126/science.1185782.

Nickerson, C., M. Harper, C. Henrie, R. Mayberry, S. Shimmin, B. Smith, and J. Smith. 2015. Land use and land cover estimates for the United States. Report prepared for the Interagency Council on Agricultural and Rural Statistics, subcommittee of the Interagency Council on Statistical Policy. https://www.ers.usda.gov/abouters/partnerships/strengthening-statistics-through-the-icars/land-use-and-land-cover-estimates-for-the-united-states/.

Piecuch, C., S. Dangendorf, R. Ponte, and M. Marcos. 2016. Annual sea level changes on the North American Northeast Coast: Influence of local winds and barotropic motions. *Journal of Climate* 29: 4801–4816. https://doi.org/10.1175/JCLI-D-16-0048.1.

Pirazzoli, P.A. 2000. Surges, atmospheric pressure and wind change and flooding probability on the Atlantic coast of France. *Oceanologica Acta* 23: 643–661. https://doi.org/10.1016/S0399-1784(00)00122-5.

Sabo, R.D., B. Sullivan, C. Wu, E. Trentacoste, Q. Zhang, G.W. Shenk, G. Bhatt, and L.C. Linker. 2022. Major point and nonpoint sources of nutrient pollution to surface water have declined throughout the Chesapeake Bay watershed. *Environmental Research Communications* 4: 045012. https://doi.org/10.1088/2515-7620/ac5db6.

Selbig, W. 2016. Evaluation of leaf removal as a means to reduce nutrient concentrations and loads in urban stormwater. *Science of the Total Environment* 571: 124–133. https://doi.org/10.1016/j.scitotenv.2016.07.003.

Shen, J., and W. Gong. 2009. Influence of model domain size, wind directions and Ekman transport on storm surge development inside the Chesapeake Bay: a case study of extratropical cyclone Ernesto, 2006. *Journal of Marine Systems* 75: 198–215. https://doi.org/10.1016/j.jmarsys.2008.09.001.

Shen, Y., M.M. Morsy, C. Huxley, N. Tahvildari, and J.L. Goodall. 2019. Flood risk assessment and increased resilience for coastal urban watersheds under the combined impact of storm tide and heavy rainfall. *Journal of Hydrology* 579: 124159. https://doi.org/10.1016/j.jhydrol.2019.124159.

Sisson, G. M.. 1976. A numerical model for the prediction of tides and tidal currents in the Lafayette River, Norfolk, Virginia. Master of Science Thesis, Ocean & Earth Sciences, Old Dominion University. https://doi.org/10.25777/57xw-ax59

Solorzano, L. 1969. Determination of ammonia in natural waters by phenolhypochlorite method. *Limnology and Oceanography* 14: 799–801. https://doi.org/10.4319/lo.1969.14.5.0799.

Spanger-Siegfried, E., M.F. Fitzpatrick, and K. Dahl. 2014. Encroaching tides: how sea level rise and tidal flooding threaten U.S. East and Gulf Coast communities over the next 30 years. Cambridge, MA: Union of Concerned Scientists. University of Minnesota Digital Conservancy. https://hdl.handle.net/11299/189228

Tu, J. 2011. Spatially varying relationships between land use and water quality across an urbanization gradient explored by geographically weighted regression. *Applied Geography* 31: 376–392. https://doi.org/10.1016/j.apgeog.2010.08.001.

Tuholske, C., B.S. Halpern, G. Blasco, J.C. Villasenor, M. Frazier, and K. Caylor. 2021. Mapping global inputs and impacts from human sewage in coastal ecosystems. *PLoS ONE* 16: e0258898. https://doi.org/10.1371/journal.pone.0258898.

van den Hurk, B., E. van Meijgaard, P. de Valk, K.J. van Heeringen, and J. Gooijer. 2015. Analysis of a compounding surge and precipitation event in the Netherlands. *Environmental Research Letters* 10: 035001. https://doi.org/10.1088/1748-9326/10/3/035001.

Virtanen, P., R. Gommers, T.E. Oliphant, et al. 2020. SciPy 1.0: Fundamental algorithms for scientific computing in Python. *Nature Methods* 17: 261–272. https://doi.org/10.1038/s41592-019-0686-2.

Wainger, L.A. 2012. Opportunities for reducing total maximum daily load (TMDL) compliance costs: Lessons from the Chesapeake Bay. *Environmental Science and Technology* 46: 9256–9265. https://doi.org/10.1021/es300540k.

Xu, K., C. Ma, J. Lian, and L. Bin. 2014. Joint probability analysis of extreme precipitation and storm tide in a coastal city under changing environment. *PLoS ONE* 9: e109341. https://doi.org/10.1371/journal.pone.0109341.

Yadav, A., and J. Pandey. 2017. Contribution of point sources and non-point sources to nutrient and carbon loads and their influence on the trophic status of the Ganga River at Varanasi. *India. Environmental Monitoring and Assessment* 189: 475. https://doi.org/10.1007/s10661-017-6188-8.

Zou, L., Y. Liu, Y. Wang, and X. Hu. 2020. Assessment and analysis of agricultural non-point source pollution loads in China: 1978–2017. *Journal of Environmental Management* 263: 110400. https://doi.org/10.1016/j.jenvman.2020.110400.